Increasing frequency of extreme La Niña events induced by greenhouse warming

Wenju Cai[1,2,], Guojian Wang[1,2], Agus Santoso[3], Michael J. McPhaden[3], Lixin Wu[2], Fei-Fei Jin[5], Axel Timmermann[6] , Mat Collins[7], Gabriel Vecchi[8], Matthieu Lengaigne[9], Matthew H. England[3], Dietmar Dommenget[10], Ken Takahashi[11], Eric Guilyardi[9,12]

1. CSIRO Marine and Atmospheric Research, Aspendale, Victoria, Australia
2. Physical Oceanography Laboratory, Qingdao Collaborative Innovation Center of Marine Science and Technology, Ocean University of China, Qingdao, China
3. Australian Research Council (ARC) Centre of Excellence for Climate System Science, Level 4 Mathews Building, The University of New South Wales, Sydney 2052, Australia.
4. NOAA/Pacific Marine Environmental Laboratory, Seattle, Washington, USA
5. Department of Meteorology, SOEST, University of Hawaii, Honolulu, Hawaii, USA
6. IPRC, Department of Oceanography, SOEST, University of Hawaii, Honolulu, Hawaii, USA
7. College of Engineering Mathematics and Physical Sciences, Harrison Building, Streatham Campus, University of Exeter, Exeter, UK
8. Geophysical Fluid Dynamics Laboratory/NOAA, Princeton, New Jersey, USA
9. Laboratoire d'Océanographie et du Climat: Expérimentation et Approches Numériques (LOCEAN), IRD/UPMC/CNRS/MNHN, Paris, France
10. School of Mathematical Sciences, Monash University, Clayton, VIC, Australia
11. Investigación en Variabilidad y Cambio Climático, Instituto Geofísico del Perú
12. NCAS-Climate, University of Reading, Reading, UK

Wenju Cai: Wenju.Cai@csiro.au
Guojian Wang: guojian.wang@csiro.au
Agus Santoso: a.santoso@unsw.edu.au
Michael J. McPhaden: michael.j.mcphaden@noaa.gov
Lixin Wu: lxwu@ouc.edu.cn
Fei-Fei Jin: jff@hawaii.edu
Axel Timmermann: axel@hawaii.edu
Mat Collins: M.Collins@exeter.ac.uk
Gabriel Vecchi: gabriel.a.vecchi@noaa.gov
Matthieu Lengaigne: Matthieu.Lengaigne@locean-ipsl.upmc.fr
Matthew England: m.england@unsw.edu.au
D. Dommenget dietmar.dommenget@monash.edu
Ken Takahashi: ken.takahashi.igp@gmail.com
Eric Guilyardi: Eric.Guilyardi@locean-ipsl.upmc.fr

The El Niño Southern Oscillation (ENSO) is Earth's most prominent source of interannual climate variability, switching irregularly between the El Niño warm phase and the La Niña cold phase, resulting in global disruption of weather patterns, ecosystems, fisheries, and agriculture (1Ropelewski and Halper 1987; 2Bove et al. 1998; 3Changnon 1999; 4Bell et al. 1999; 5McPhaden et al. 2006). The 1998/99 extreme La Niña that followed the 1997/98 super El Niño event (6McPhaden), switched extreme El Niño-induced severe droughts to devastating floods in western Pacific countries, and El Niño-induced catastrophic floods to severe drought in southwest of US (4Bell et al. 1999; 7Hoerling and Kumar 2003). Although recent discoveries have revealed robust changes in El Niño and its impacts under greenhouse warming (8Cai et al. 2014; 9Power et al. 2013; 10Santoso et al. 2013), the response of La Niña events are yet to be examined. Here we present climate modelling evidence for a near doubling in the frequency of extreme La Niña. About half of the projected increase occurs in the year following an extreme El Niño, thus projecting more frequent climatic swings of opposite extremes from one year to the next, analogous to the 1997-1998 extreme episodes. We estimate these changes by aggregating results from climate models in the Coupled Model Intercomparison Project phases 5 (CMIP5) multi-model databases (11Taylor 2013). During an extreme La Niña, coldest anomalies are situated in the central Pacific (12Dommenget), generating an enhanced east-minus-west anomalous sea surface temperature (SST) gradient along the equator, a commonality shared by an extreme El Niño. We find that this enhanced gradient is supported by a La Niña Modoki (13Ashok et al. 2007), with cold SST anomaly situated in the central equatorial Pacific and warm anomaly in the east. Greenhouse warming strengthens such a gradient in the mean state, thus facilitating increased occurrences of extreme La Niña, as well as extreme El Niño events.

Impact of La Niña in general. During moderate La Niña events, the eastern equatorial Pacific is colder than normal, opposite to that of El Niño events. This inhibits formation of rain-producing clouds there, but enhancing atmospheric convection and rainfall elsewhere, particularly in the equatorial western Pacific. The associated atmospheric circulation changes, such as in 1985 (Fig. 1a), spurred extreme weather in many parts of the world, including droughts in Southwest United States (1Ropelewski and Halper 1987; 14Kiladis and Diaz; 1989) and eastern equatorial Pacific regions, floods in the western Pacific and central American countries (1Ropelewski and Halper 1987; 15Hoyos et al. 2013), and increased land-falling West Pacific cyclones and Atlantic hurricanes (16Wu el al. 2004; 2Bove et al. 1998; 17Gray 1984).

Impacts of extreme La Niña. The SST anomaly patterns, and the associated impacts, however, differ vastly from event to event. The difference in pattern between the moderate La Niña in 1985 and the 1998 extreme event, for instance, is striking (Fig. 1a, b). During the 1998 event, the cold SST anomalies peak notably farther west, in the central equatorial Pacific, generating an east-minus west SST gradient, accompanied by a stronger and meridionally broader western tropical Pacific warm pool (Fig. 1b, Extended Fig. 1). Consequently, the centre of dry anomalies is situated in the western and central Pacific and wet anomalies expand meridionally (Extended Data Fig. 1). The impact of the associated convection changes is global in scale. There was complete disappearance of rainfall across the east-central equatorial Pacific. Southwest US experienced one of the most severe droughts in history (7Hoerling and Kumar 2003; 4Bell et al. 1999; 18Cole 2002). Venezuela endured flash flood and landslide that killed an estimated 25,000 to 50,000 people (19Takahashi et al. 2001). In China, river floods and storms led to the death of thousands, and displacement of over 200 million people (20Jonkman 2005). Bangladesh experienced one of the most destructive flooding events in modern world history, with over 50% of the land

94 flooded, severe food shortage and massive water-borne epidemic diseases, killing several
95 thousand people and affecting over 30 million more (21Kunii et al. 2002; 22del Ninno 2001;
96 23Mirza, 2001). The 1998 North Atlantic hurricane season was far more active than normal,
97 and saw one of the deadliest and strongest hurricanes (Mitch) in the historical record (4Bell et
98 al. 199); in Honduras and Nicaragua, the associated extreme floods and mudslides claimed
99 more than 11,000 lives (24Kerle et al. 2002).

100 **Transition to Science.** The 1998 La Niña event occurred in the year following the 1997
101 extreme El Niño event – an event considered as the climate event of the 20th Century
102 (3Changnon 1999), followed immediately in 1999 by another extreme La Niña, causing
103 prolonged impacts. Another extreme La Niña occurred earlier in 1988 following the two-year
104 long moderate 1986-88 El Niño, with dire consequences. Recent studies have shown a
105 greenhouse warming-induced increase in extreme El Niño events (8Cai et al. 2014), El Niño
106 with eastward-propagating SST anomalies (10Santoso et al. 2013), or with a drastic swing of
107 the South Pacific Convergence Zone toward the equator (25Cai et al. 2012), but how La Niña
108 events will change in a warming climate has not been systematically examined. The severe
109 impacts described above call for an examination of this issue. Here we show that greenhouse
110 warming leads to a near doubling in the frequency of extreme La Niña.

111 **Characterization of extreme La Niña**. The vastly different anomaly pattern between an
112 extreme and moderate La Niña (Figs 1a-b) suggests that ENSO dynamics is nonlinear and its
113 depiction requires more than one index (11Dommenget, 26Takahashi,). Only considering the
114 Niño3 index (SST anomalies over 150^{o}W-90^{o}W, 5^{o}S-5^{o}N) would imply an identical anomaly
115 pattern differing only in the intensity. To capture the nonlinearity, we apply an Empirical
116 Orthogonal Function (EOF) analysis to deconvolve the spatio-temporal SST variability into
117 orthogonal modes, each described by a principal spatial pattern and an associated principal
118 component time series (See Methods Lorenz 1956). We focus on satellite-era observations

(See Methods, Adler, Balmaseda), and austral summer (December to February) when a La Niña peaks.

At their positive phase, the first EOF (Fig. 1c), showing a canonical La Niña pattern, and the second EOF, a La Niña Modoki pattern (13Ashok et al. 2007) (Fig. 1d), are highly correlated with Niño3 (r=0.98) and with an ENSO Modoki index (13Ashok et al. 2007) (r=0.82), respectively. The two time series display a strong "V-shaped" nonlinear relationship (Fig. 1e).

The 1998 extreme La Niña manifested as a strong La Niña Modoki (EOF2) superimposed on a canonical La Niña (EOF1) (Extended Data Fig. 2), such that maximum cold anomalies in the west and central Pacific are accompanied by large and broad positive SST anomalies over the far western Pacific (Fig.1b). In contrast, the 1985 moderate La Niña is the difference between the appropriately weighted EOF1 and EOF2 (Extended Fig. 2), such that the maximum cool anomalies are situated in the eastern equatorial Pacific (Fig. 1b). The 1982/83 and 1997/98 extreme El Niño events manifested as a superimposition of a strong canonical El Niño (EOF1) and a strong La Niña Modoki (EOF2) (Fig. 1e), with warm anomalies in far eastern equatorial Pacific, such that the warmest SST is located in the eastern equatorial Pacific (8Cai).

Thus, the La Niña Modoki equatorial SST gradient emerges as a commonality embedded in both an extreme El Niño and extreme La Niña, which, as we will show, acts as an amplifier to canonical El Niño and La Niña, turning them into extreme events. A La Niña Modoki features cold anomalies in the central Pacific but warm SST anomalies in the eastern Pacific (Fig. 1d). SST and wind anomalies of a canonical La Niña are offset in the eastern but strengthened in the central equatorial Pacific by La Niña Modoki anomalies, giving rise to a cold anomaly that peaks in the western and central Pacific and an ***enhanced east-minus-west***

143 ***SST gradient*****,** characterising an extreme La Niña (Fig. 2a). Conversely, warm anomalies of a
144 canonical El Niño are offset in the central Pacific, but strengthened in the eastern Pacific,
145 giving rise to a warm anomaly peaking in the eastern Pacific (Fig. 2b) and an ***enhanced east-***
146 ***minus-west SST gradient****,* the hallmark of an extreme El Niño (8Cai et al. 2014). By contrast,
147 an El Niño Modoki damps a canonical El Niño or La Niña (Fig. 2c, d), and a strong El Niño
148 Modoki tends to occur independently of canonical ENSO events. These features are
149 evidenced by the "V-shaped" nonlinear relationship (Fig. 1e).

150 This functionality of a La Niña Modoki amplifying a La Niña or El Niño can be directly
151 depicted by an equatorial zonal SST anomaly gradient (Fig. 1f), defined as SST anomalies
152 averaged over the eastern (5^oS-5^oN, 80^oW-90^oW) minus that over the central (5^oS-5^oN,
153 160^oE-210^oE) equatorial Pacific. This ENSO "Amplifier" index, has a correlation with the
154 SST EOF2 of 0.97 (Fig. 1f): a large positive value corresponding to a strong La Niña
155 Modoki. Under greenhouse warming, this index trends upward due to a faster warming in
156 the eastern than the western equatorial Pacific (27Xie 2010).

157 We define an extreme La Niña as one for which the amplitude of EOF1 is greater than a one-
158 standard deviation value, and EOF2 greater than a 0.75-standard deviation value. This
159 definition captures the three extreme La Niña austral summers of 1988, 1998, and 1999.
160 Since a La Niña tends to last for more than one year (18Cole 2000), the 1998 and 1999
161 conditions are counted as one event, as they are both preceded by a discharged equatorial
162 Pacific upper ocean heat content due to the 1997/98 El Niño (28Jin 1997). Indeed, most La
163 Niña events, consecutive or otherwise occur following a discharged heat marked by a
164 shallowing of thermocline depth across the equatorial Pacific. The same EOF definition
165 identifies the two well-known extreme El Niños of 1982/83 and 1997/98.

166 An identical analysis on observed rainfall anomalies produces two EOFs that are similarly
167 nonlinearly related, and identifies the same extreme El Niño and La Niña events (Extended
168 Data Fig. 3). The first and second rainfall EOFs correspond to the first and second SST
169 EOFs, with a correlation between the two corresponding EOFs at 0.94 and 0.88, respectively
170 Further, the rainfall EOF2 also varies coherently with the Amplifier index, with a correlation
171 of 0.89 (Extended Data Fig. 3f).

172 **Response to greenhouse warming.** We select 17 CMIP5 models that are able to simulate
173 nonlinear process associated with extreme ENSO events, identified using rainfall skewness
174 and ability to generate extreme El Niño events (8Cai et al. 2014) (see Methods). These
175 coupled general circulation models (CGCMs) are forced with historical anthropogenic and
176 natural forcings, and future greenhouse gas emission scenarios, covering the 1900-2099
177 period. The models reproduce the nonlinear relationship between the two EOFs, confirming
178 their ability to simulate extreme El Niño and extreme La Niña events. We define an extreme
179 La Niña event in the same manner as in the observed, and compare the frequency in the first
180 (1900–1999) and second (2000–2099) 100-year periods, referred to as the *Control* and
181 *Climate Change* periods, respectively.

182 Based on rainfall EOFs, the frequency of extreme La Niña events doubles from about one
183 event every 24 years (70 events in 1,700 years) in the *Control,* to one every 12 years (143
184 events in 1,700 years) in the *Climate Change* period (Fig. 3a-3d). The increase is statistically
185 significant according to a bootstrap test (Austin), underscored by a strong inter-model
186 consensus (see Methods), with 1 out of 17 models simulating a decrease (Extended Data
187 Tables 1). Sensitivity tests to varying definitions of extreme La Niña (e.g., using different
188 combination of EOF1 and EOF2 value) further support the robustness of this result (Extended
189 Table 1). In terms of extreme El Niño events, our definition consistently produces a 67%
190 increase in occurrences with 12 out of 17 models producing an increase, a reasonably strong

191 inter-model consensus. Thus under greenhouse warming, both extreme La Niña and extreme
192 El Niño increases in frequency. 42% of the increased extreme La Niña events occur in the
193 year following an extreme El Niño event.

194 Results based on SST EOFs are similar (Fig. 3e-h) (Extended Data Fig. 4), though the
195 increase is smaller, by 53%, with 12 out 17 (70%) models agreeing for extreme La Niña
196 events, compared to an increase of 35% with 11 out of 17 models (65%) agreeing for
197 extreme El Niño events (Extended Data Table 4). About 60% of the increased La Niña events
198 occur in the year following an extreme El Niño event. The smaller increases compared to
199 those based on rainfall EOFs are expected, since under greenhouse warming rainfall
200 anomalies are more sensitive to SST anomalies (29Chung and Power, 8Cai et al. 2014)
201 (Extended Data Fig. 4). In terms of impact most relevant to society, rainfall is a better
202 indicator for ENSO activity (Cai et al. 2014). Thus, the rainfall-based results should be
203 highlighted in the consideration for future projections.

204 **Telconnection.** In most regions, differences in extreme La Niña rainfall teleconnection
205 pattern between the *Control* and *Climate Change* period (left column, Extended Data Fig. 5)
206 are not statistically significant, with the exception of some western Pacific regions, e.g.,
207 northern Australia (Extended Data Fig. 6), where anomalies are greater in the *Climate*
208 *Change* period. Given the large increase in frequency, this suggests that in general the
209 impacts of extreme La Niña events experienced in the *Control* period will repeat more
210 frequently in the *Climate Change* period.

211 **Mechanism.** The increased frequency of extreme El Niño and extreme La Niña relies on an
212 increase in occurrences of strong Modoki La Niña (EOF2), that is, an increase in events with
213 a strong Amplifier. Time series of Amplifier index (east-minus-west SST gradient) across
214 the models display a strong correlation (r=0.73, with 3400 samples) with SST EOF2 (Fig.

4a). Large values tend to occur with extreme El Niño and La Niña events and are located in the same quadrant. Thus the model SST EOF2 can be represented by the Amplifier index, as in the observations (Fig. 1f). The raw index shows an increase in the frequency of large values (Extended Data Fig. 7a, b), because under greenhouse warming, the equatorial east-minus-west zonal SST gradient intensifies (Fig. 4b), due to a faster warming in the eastern equatorial Pacific than in the west (27Xie et al. 2010). This trend translates into more frequent occurrences of events with a strong Amplifier (Fig. 4c) and with a larger SST and rainfall EOF2, see Extended Data Fig. 7), hence more-frequent extreme La Niña events (Fig. 4c). In other words, as the eastern Pacific mean climate warms faster than the west, it takes a smaller change in SST to generate an equal amount of rainfall or zonal SST gradient associated with extreme La Niña in the *Control* period. There is also a tendency for an increase in the frequency of strong canonical La Niña events that can be amplified into extremes, as evidenced by a spread toward large positive EOF1 values (Fig. 3e, f). For example, events with EOF1 >1.5 increase by 14%. The increase is in part associated with a shallowing trend in the mean thermocline (30Vecchi et al. 2007), which leads to a higher sensitivity of SST to the thermocline anomalies (Extended Data Fig. 8).

In summary, our result of a greenhouse-induced increase in occurrences of extreme La Niña events is consistent with previous findings of an increase in extreme El Niño events because they are both facilitated by the same amplifier, a Modoki-La Niña, embedded in the equatorial east-minus-west SST gradient. Greenhouse warming leads to an increase in the gradient of the mean state, hence more occurrences for a given amplification strength. The overall increased frequency, and the large portion of the increase that occur in the year after an extreme El Niño, means that there will be more occurrences of devastating weather events, and more-frequent swings of opposite extremes from one year to the next, with profound implications for the 21st century.

240 **Methods Summary**

241 The extreme La Niña events were diagnosed using a suite of distinctive process-based
242 indicators, such as the position of maximum equatorial easterly, cold, and low rainfall
243 anomalies, which is situated at the western Pacific during an extreme La Niña, as opposed to
244 the eastern equatorial Pacific during moderate La Niña. For observations, we focus on
245 historical events in the satellite era (1979–present) monthly precipitation analysis SSTs and
246 other circulation fields from a global reanalysis (see Methods). We focus on austral summer,
247 December-February (DJF) in which a La Niña typically peaks. The vastly different anomaly
248 pattern between moderate and extreme La Niña suggests that the traditional index, e.g.,
249 Niño3 defined SST anomalies over (150°W-90°W and 5°S-5°N) is not sufficient to
250 differentiate an extreme La Niña from a moderate one. Thus, we propose an identification
251 method for extreme La Niña, in which we apply EOF analysis to rainfall and SST anomalies
252 in the equatorial Pacific Ocean. This produces two principal variability patterns, one
253 depicting a canonical La Niña and the other resembling a La Niña Modoki (13Ashok),
254 display a nonlinear relationship. An extreme La Niña event is defined as when the first
255 principal time series is greater than one standard deviation and the second greater than a 0.75
256 standard deviation. This definition captures the 1988 and 1998 observed extreme La Niña
257 events. To select CGCMs, we use criteria of positive rainfall skewness in the eastern
258 equatorial Pacific greater 1 and ability to simulate extreme events as in Ref. 8 (8Cai et al.
259 2014). The method selects 17 CMIP5 CGCMs, each covering 105 years of a pre-21st
260 century climate change simulation using historical anthropogenic and natural forcings (1901-
261 2005) and a further 95 years (2006-2100) under the RCP8.5 forcing scenario
262 (12Taylor2014).

263

References

1. Ropelewski, C. F., and Halpert, M. S. Global and regional scale precipitation patterns associated with the El Niño/Southern Oscillation. *Mon. Wea. Rev.,* **115,** 1606–1626 (1987).
2. Bove, M. C., O'Brien, J. J., Eisner, J. B., Landsea, C. W. & Niu, X. Effect of El Niño on U.S. landfalling hurricanes, revisited. Bull. Amer. *Meteor. Soc.* **79**, 2477–2482 (1998).
3. Changnon, S. A., Impacts of 1997—98 El Niño generated weather in the United States. *Bull. Amer. Meteor. Soc*. **80,** 1819–1827 (1999).
4. Bell, G. D. et al. Climate Assessment for 1998. Bull. *Amer. Meteor. Soc*. **80,** 1040–1040 (1999).
5. McPhaden, M. J., Zebiak, S.E. & Glantz, M. H. ENSO as an integrating concept in Earth science. *Science* **314**, 1740-1745 (2006).
6. McPhaden, M. J. El Niño: The child prodigy of 1997–98. *Nature* **398**, 559–562. doi:10.1038/19193 (1999).
7. Hoerling, M. & Kumar, A. The Perfect Ocean for Drought. *Science* **299,** 691-694 (2003).
8. Cai, W., S. Borlace, M. Lengaigne, P. van Rensch, M. Collins, G. Vecchi, A. Timmermann, A. Santoso, M. J. McPhaden, L. Wu, M. H. England, G. Wang, E. Guilyardi, and F.-F. Jin (2013) Increasing frequency of extreme El Niño events due to greenhouse warming. *Nature Climate Change,* **4,** 111-116, 2014 | doi: 10.1038/nclimate2100 (2014).
9. Power, S., Delage, F., Chung, C., Kociuba, G. & Keay, K. Robust twenty-first-century projections of El Niño and related precipitation variability. Nature 502, 541-545 (2013).
10. Santoso, A., S. McGregor, F.-F. Jin, W. Cai, M. H. England, S.-I. An, M. J. McPhaden, & E. Guilyardi (2013) Late-twentieth-century emergence of the El Niño propagation asymmetry and future projections. *Nature,* **504,** 126–130. doi:10.1038/nature12683 (2013).
11. Dommenget, D. Bayr, T., & Frauen, C. Analysis of the non-linearity in the pattern and time evolution of El Niño southern oscillation. *Clim. Dyn.* **40**, 2825–2847. DOI 10.1007/s00382-012-1475-0 (2013).

290 12. Taylor, K. E., Stouffer, R. J. & Meehl, G. A. An overview of CMIP5 and the experimental
291 design. *Bull. Amer. Met. Soc*. **93,** 485–498, doi: 10.1175/BAMS-D-11-00094.1 (2012).
292 13. Ashok, K., Behera, S. K., Rao, S. A., Weng, H. & Yamagata, T. El Niño Modoki and its
293 possible teleconnection. *J. Geophys. Res.* **112,** C11007, doi:10.1029/2006JC003798 (2007).
294 14. Kiladis G. N. and Diaz, H. F. Global climate anomalies associated with extremes in the
295 Southern Oscillation. *J. Clim.* **2,** 1069-1090 (1989)
296 15. Hoyos, N., Escobar, Restrepo, J. C., Arango, A. M., and Ortiz, J. C. Impact of the 2010e2011
297 La Niña phenomenon in Colombia, South America: The human toll of an extreme weather
298 event. *Applied Geography* **39**, 16-25 (2013)
299 16. Wu, M. C., Chang, W. L., and Leung, W. M. Impact of El Niño-Southern Oscillation Events
300 on tropical cyclone landfalling activities in the western North Pacific. *J. Clim.* **17,** 1419-1428
301 (2004).
302 17. Gray, W. M., 1984: Atlantic seasonal hurricane frequency: Part I: El Niño and 30-mb
303 quasibiennial oscillation influences. *Mon. Wea. Rev.,* **112,** 1669–1683.
304 18. Cole, J. E., and Overpeck, T. Multiyear La Niña events and persistent drought in the
305 contiguous United State. *Geophs. Res. Lett.,* **29,** 1647, 10.1029/2001GL013561 (2002).
306 19. Takahashi, T. Nakagawa, H., Satofuka, Y. and Kawaike, K. Flood and sediment disasters
307 triggered by 1999 rainfall in Venezuela; A River Restoration Plan for an Alluvial Fan. Journal
308 of Natural Disaster. *Science,* **23**, 65-82 (2001).
309 20. Jonkman, S. N. Global Perspectives on Loss of human life caused by floods. *Natural Hazards*
310 **34,** 151–175 (2005).
311 21. Kunii, O. Nakamura, S., Abdur, R., and Wakai, S.The impact on health and risk factors of
312 the diarrhoea epidemics in the 1998 Bangladesh floods. *Public Health* **116,** 68–74 (2002).
313 22. del Ninno, C., & Dorosh, P. A. Averting a food crisis: private imports and public targeted
314 distribution in Bangladesh after the 1998 flood. *Agricultural Economics* **25,** 337-346 (2001).
315 23. Mirza, M. M. Q., Warrick, R. A., Ericksen, N. J., & Gavin, G. J. Are floods getting worse in
316 the Ganges, Brahmaputra and Meghna basins? *Environmental Hazards* **3,** 37–48 (2002).

24. Kerle, N., Froger, J. L., and Oppenheimer, C., and Van Wyk De Vries, B. Remote sensing of the 1998 mudflow at Casita volcano, Nicaragua. *International Journal of Remote Sensing* **24,** 4791-4816 (2003)

25. Cai, W., M. Lengaigne, S. Borlace, M. Collins, T. Cowan, M. J. McPhaden, A. Timmermann, S. Power, J. Brown, C. Menkes, A. Ngari, E. M. Vincent, and M. J. Widlansky (2012) More extreme swings of the South Pacific Convergence Zone due to greenhouse warming. *Nature* **488,** 365–369. doi:10.1038/nature11358 (2012).

26. Takahashi, K., Montecinos, A., Goubanova, K., and Dewitte, B. ENSO regimes: Reinterpreting the canonical and Modoki El Niño, *Geophys. Res. Lett.,* **38**, L10704, doi:10.1029/2011GL047364 (2011).

27. Xie, S. P. et al. Global warming pattern formation: sea surface temperature and rainfall. *J. Clim.* **23,** 966–986 (2010).

28. Jin, F. F. An equatorial ocean recharge paradigm for ENSO .1. Conceptual model. *J Atmos Sci.* **54,** 811-829 (1997).

29. Chung, C. T. Y. and Power, S. B. Precipitation response to La Niña and global warming in the Indo-Pacific. *Climate Dynamics.* 10.1007/s00382-014-2105-9 (2014).

30. Vecchi, G.A., & Soden, B.J. Global warming and the weakening of the tropical circulation. *J. Clim.* **20,** 4316–4340 (2007).

Acknowledgements

W. C. and G. W. are supported by the Australian Climate Change Science Program and a CSIRO Office of Chief Executive Science Leader award. A.S. is supported by the Australian Research Council. ….

Author Contributions

W.C. conceived the study and directed the analysis. G. W. performed the model output analysis. W. C. wrote the initial draft of the paper. All authors contributed to interpreting results, discussion of the associated dynamics, and improvement of this paper.

Author Information Reprints and permissions information are available at:

www.nature.com/reprints. The authors declare no competing financial interests. Correspondence and requests for materials should be addressed to Wenju Cai (wenju.cai@csiro.au).

Figure Legends

Figure 1 | (to be inserted)

Methods

Data, reanalyses, and EOF analysis

We utilised data in the satellite era (1979–present) which include Global Precipitation Climatology Project monthly precipitation analysis (31Adler) http://www.esrl.noaa.gov/psd/data/gridded/data.gpcp.html, global analyses of SSTs (32Balmaseda), and circulation fields from the National Center for Environmental Prediction (NCEP) and National Center for Atmospheric Research (NCAR) global reanalysis (33JKalnay). We use a multivariate signal processing method referred to as EOF analysis (34Lorenz) to deconvolve the spatio-temporal variability into orthogonal modes, each described by a principal spatial pattern and an associated principal component time series.

363 The EOF analysis is applied to both rainfall and SST anomalies, referenced to the mean since
364 1979 for the observed, and mean the *Control* period for the model outputs with anomalies
365 covering the entire 200-year period. For SST, we use an equatorial domain (15^oS-15^oN,
366 140^oE-280^oE), but for rainfall, an equatorial domain (5^oS-5^oN, 140^oE-280^oE) to highlight
367 concentrated convective variability along the equator (Fig. 1b). Model SST anomalies
368 display a distinctive warming trend manifested as the first EOF mode and this is removed
369 first. To facilitate easy discussion, SST EOF1 and EOF2 are actually modes after the trend
370 mode are removed. In contrast, model rainfall anomalies show no such trends. Before used
371 to identify extreme events, all EOF time series are quadratically detrended to ensure no trend
372 is present.

373 **Characterization of extreme La Niña events**

374 The extreme La Niña events were diagnosed using a suite of distinctive process-based
375 indicators, such as anomaly centre of equatorial easterly, cold, and low rainfall anomalies,
376 which is situated at the western Pacific during extreme La Niña, as opposed to the eastern
377 equatorial Pacific during moderate La Niña. The difference in spatial pattern is captured by
378 different combination of two principal variability patterns. The EOF1 reflects a canonical La
379 Niña pattern embedded in the commonly used Niño3 index, featuring cool and dry anomalies
380 extending from the eastern equatorial Pacific to the central Pacific. The EOF2 resembles the
381 La Niña Modoki pattern (13 Ashok), featuring a cool and dry anomalies in the central Pacific
382 but warm and wet anomalies in the eastern equatorial Pacific. An extreme La Niña is an
383 appropriately weighted superimposition of the two patterns, giving rise to anomaly centre in
384 the west Pacific, whereas a moderate La Niña is an appropriately weighted difference
385 between EOF1 and EOF2, leading to warmest anomalies in the eastern equatorial Pacific.

386 **East-minus-west zonal SST gradient along the equator**

An important feature of extreme La Niña events is an *enhanced* east-minus-west Pacific SST gradient along the equator, common to an extreme El Niño. This is because during extreme La Niña the cold anomaly centre is located in the central Pacific, where cold anomalies are colder than in the eastern Pacific. During extreme El Niño, warm anomalies are maximum in the eastern equatorial Pacific, generating an *enhanced* east-minus-west Pacific SST gradient along the equator, defined as an equatorial zonal SST anomaly gradient (Fig. 1f), defined as SST anomalies averaged over the eastern (5^oS-5^oN, 80^oW-90^oW) minus that over the central (5^oS-5^oN, 160^oE-210^oE) equatorial Pacific (Figs 1f, 4a).

Model Selection

We utilise 27 CMIP5 CGCMs (Supplementary Table 1) forced with historical anthropogenic and natural forcings, and future greenhouse gas under emission scenario of Representative Concentration Pathway (RCP) 8.5 (12Taylor), covering a 200-year period. Two features of the nonlinearity used to identify models for extreme El Niño (8Cai) are used to select models. These are the positive skewness of rainfall anomalies and ability to generate rainfall greater than 5 mm day^{-1} over the eastern equatorial Pacific. Although the majority of CGCMs generate ENSO-like variability, only a subgroup of CGCMs simulate the observed nonlinear ocean-atmosphere coupling over the eastern equatorial Pacific as depicted by the positive skewness of SST anomalies over the eastern pole during the austral summer (DJF), which is 2.7 in observations since 1979. The level of nonlinearity varies vastly among CGCMs, and we consider positive skewness of 1 as our threshold. Out of the 31 CGCMs, 17 models satisfy the rainfall skewness criterion. The selected CGCMs yield a mean skewness of 2.52, close to the observed (Extended Data Table 1).

All selected 17 CGCMs reproduce the observed extreme La Niña pattern. The same EOF analysis is carried out for each individual model using rainfall and SST anomalies referenced

411 to the mean over the *Control* period. Prior to the analysis, data are interpolated into a
412 common grid of 1.5 degree latitude by 1.5 degree longitude. Our EOF outputs are scaled so
413 that the EOF time series have a standard deviation of one to facilitate an inter-model
414 comparison and aggregation. All 17 models produce the nonlinear relationship between the
415 two leading EOFs, indicating their ability to generate the nonlinear equatorial positive
416 feedback associated with the extreme La Niña.

417 We derive changes in the occurrence of extreme La Niña events by comparing the frequency
418 of the first 100 years (*Control* period) to that of the second 100 years (*Climate Change*
419 period). We also test the sensitivity of our results to varying definitions (Extended Data
420 Tables 1). In all cases, there is a statistically significant increase (near doubling) in the
421 occurrences of extreme La Niña events from the *Control* to the *Climate Change* period.

422 **Statistical significance test**

423 We use a bootstrap method (35Austin) to examine whether the change in frequency of the
424 extreme La Niña events is statistically significant. The 1,700 samples from the 17 CMIP5
425 CGCMs in the *Control* period are re-sampled randomly to construct another 10,000
426 realisations of 1,700-year records. In the random re-sampling process, any extreme La Niña
427 event is allowed to be selected again. The standard deviation of the extreme La Niña
428 frequency using a rainfall definition in the inter-realisation is 7.7 events per 1,700 years, far
429 smaller than the difference of 73 events per 1,700 years between the *Climate Change* and the
430 *Control* periods (Fig. 3c, d), indicating a strong statistical significance. Using an SST
431 definition, the inter-realisation standard deviation is 8.8 events per 1,700 years, far smaller
432 than the difference of 42 events per 1,700 years between the *Climate Change* and the *Control*
433 periods (Fig. 3c, d), indicating a strong statistical significance. Increasing the realisations to
434 20,000 or 30,000 yields essentially an identical result.

Methods References

31. Adler, R. F. *et al.* The version 2 Global Precipitation Climatology Project (GPCP) monthly precipitation analysis (1979–present). *J. Hydrometeor.* **4,** 1147–1167 (2003).
32. Balmaseda, M. A., Mogensen, K. and Weaver, A. T., Evaluation of the ECMWF ocean reanalysis system ORAS4. *Q.J.R. Meteorol. Soc.,* **139,** 1132–1161. doi: 10.1002/qj.2063 (2013).
33. Kalnay, E., et al. The NCEP/NCAR 40-Year Reanalysis Project. *Bull. Amer. Meteor. Soc.,* **3,** 437-471 (1996).
34. Lorenz, E. N., Empirical orthogonal functions and statistical weather prediction. MIT Department of Meteorology, Statistical Forecast Project Rep. 1, 49 pp. (1956) [Available from Dept. of Meteorology, MIT, Massachusetts Ave., Cambridge, MA 02139.]
35. Austin, P. C. Bootstrap Methods for Developing Predictive Models. *The American Statistician.* **58,** 131-137 (2004).

Extended Data legends

To be inserted.

Figures and Legends

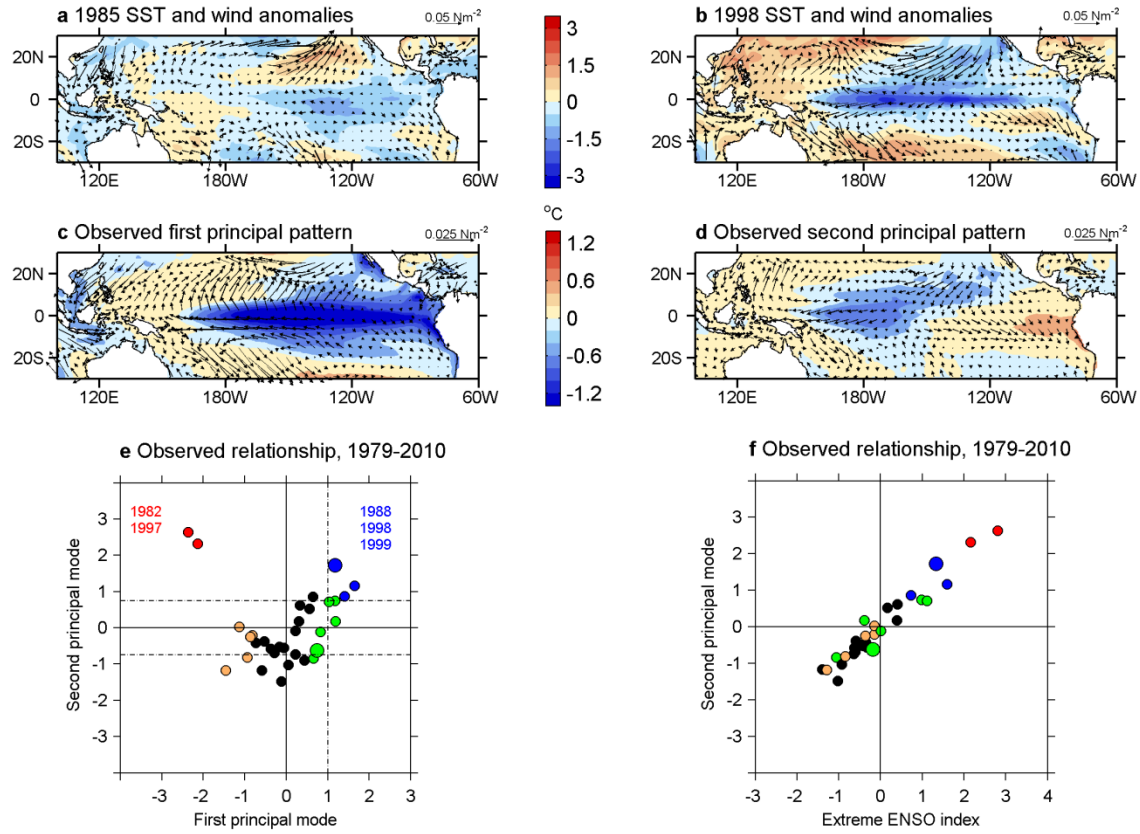

Figure 1 | Comparison of a moderate and extreme La Niña and identification of extreme La Niña events. a, b, December to February (DJF) average SST anomalies (shading, ^{o}C) and wind stress (vectors, scale shown in the top right corner for each panel) anomalies associated with a moderate (1985) and extreme (1998) extreme La Niña. **c, d,** Principal variability patterns of SST obtained by applying EOF analysis to a satellite-era SST anomalies (see Methods), in the equatorial region (15^{o}S-15^{o}N, 140^{o}E-280^{o}E). The associated SST anomalies outside the domain and wind stress vectors from reanalysis data (see Methods) are presented as linear regression onto the EOF time series. **e,** Relationship between the two principal component time series. An extreme La Niña event (**blue** dots, **big blue 1998**) is defined as when the first principal component is greater than 1.0 standard deviation (s.d.), and the second principal component is greater than 0.75 s.d. An extreme El Niño event (**red** dots) is defined as when amplitude of the first principal component is greater than 1.0 standard deviation (s.d.), and the second principal component is greater than 0.75 s.d. **Orange** dots

467 indicate **weak El Niño**, and **green** dots, **weak La Niña (big green, 1985)** defined as when
468 quadratically detrended Niño3 is greater than 0.75 s.d. in amplitude. **f,** Relationship between
469 the second principal component time series and a time series of an equatorial east-minus-west
470 anomalous SST gradient, referred as an Amplifier index, defined as an average over the east
471 (5^oS-5^oN, 80^oW-90^oW) minus that over the central Pacific (5^oS-5^oN, 160^oE-210^oE).
472

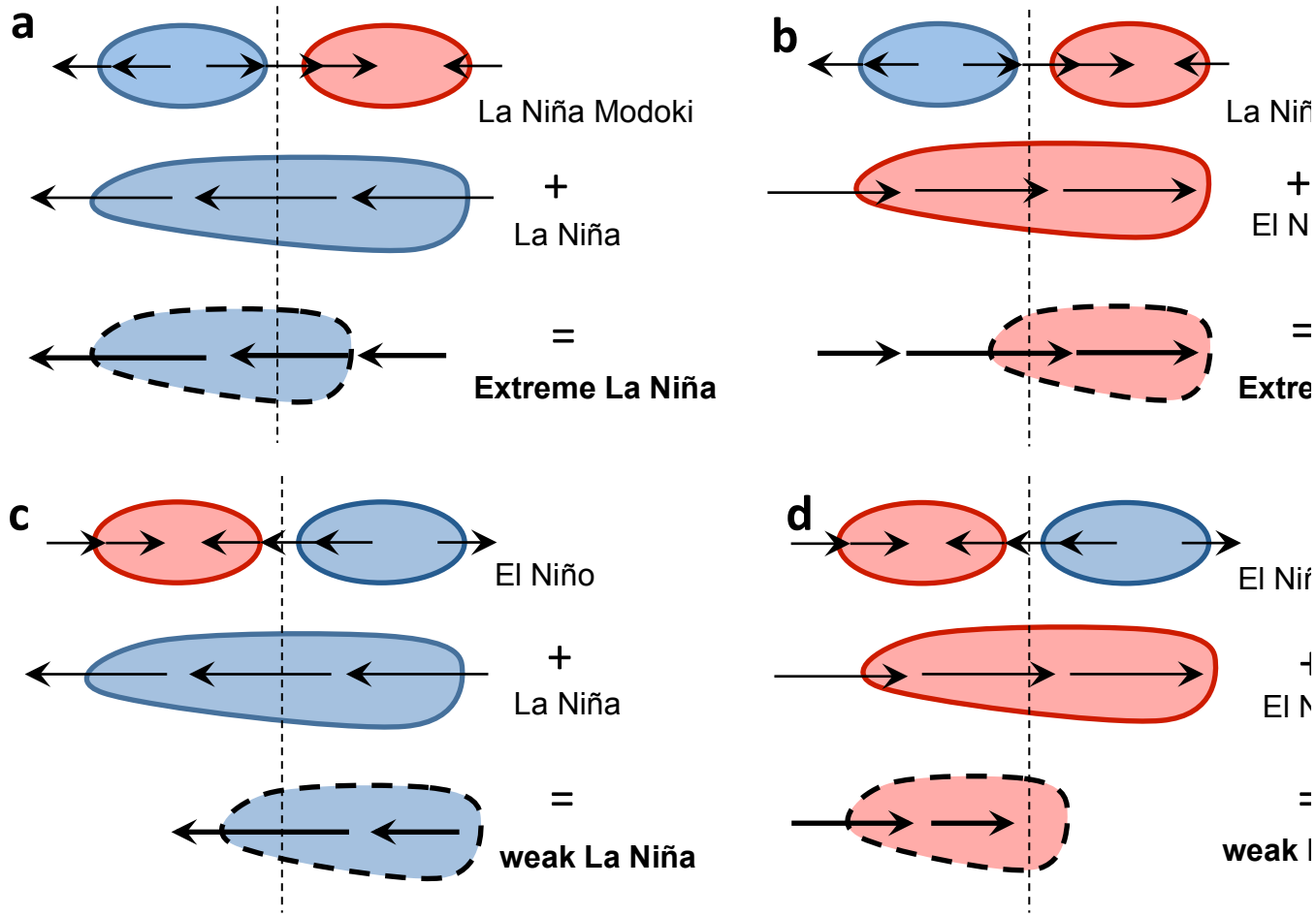

473

474 **Figure 2 | Schematic diagram of the ENSO Modoki effect on ENSO.** The effect can be
475 discerned by superimposing SST and wind anomalies associated with ENSO Modoki onto
476 those of canonical ENSO. **Red** and **blue** patterns correspond with **warm** and **cold**
477 anomalies, respectively, and arrows of different sizes denote anomalous wind anomalies of
478 relative strengths. Superimposing La Niña Modoki SST anomalies onto either canonical La
479 Niña (**a**) or El Niño (**b**) anomalies yield either extreme La Niña events characterized by large

480 cool anomalies in the central Pacific (**a**), or extreme El Niño events characterised by strong
481 SST anomalies in the eastern Pacific (**b**). In contrast, superimposing El Niño Modoki SST
482 anomalies result in either a weak La Niña (**c**) or a weak El Niño (**d**) event.

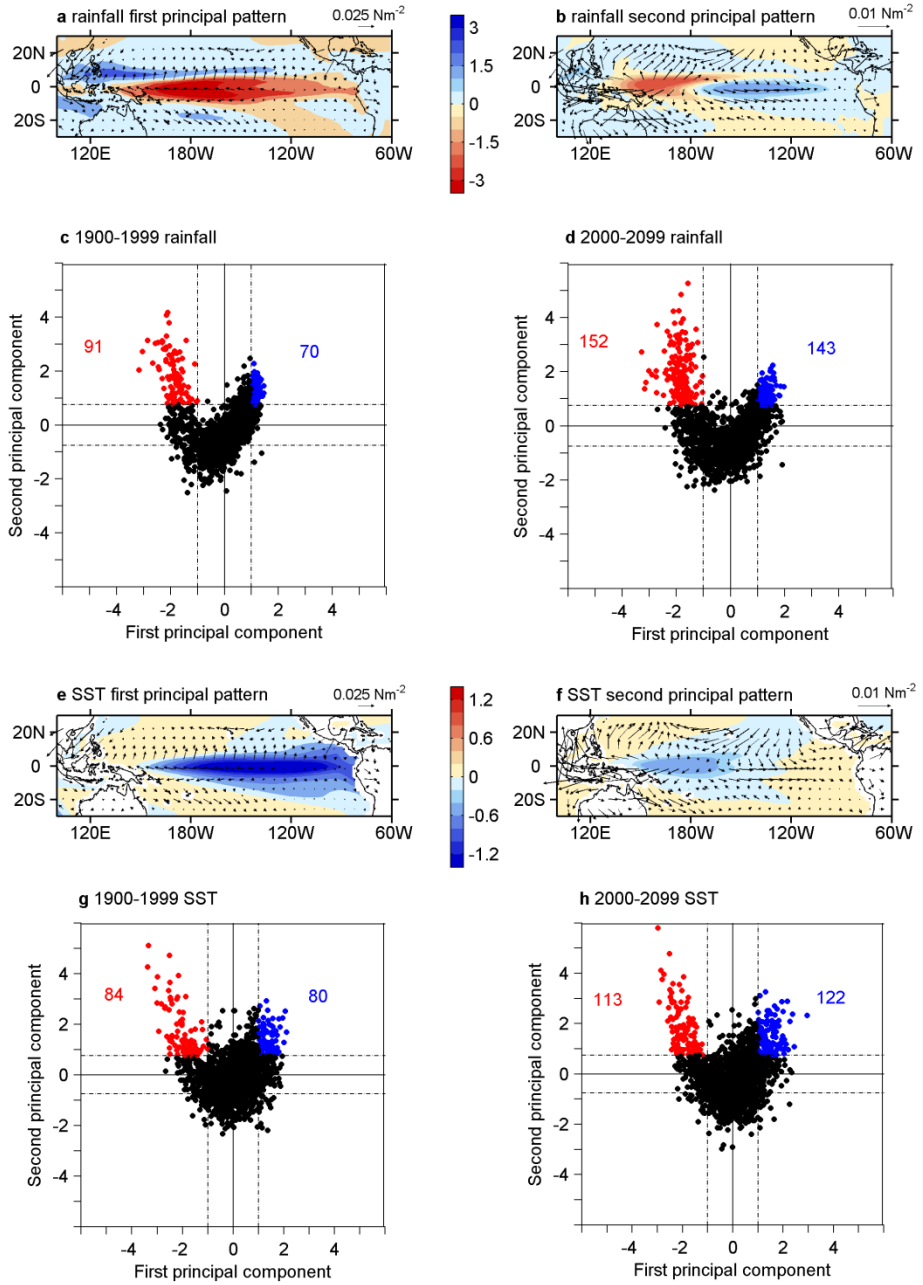

483

484 **Figure 3 | Multi-model ensemble average of the principal variability patterns of austral**
485 **summer season and their nonlinear relationship**. **a, b,** First and second principal
486 variability patterns of SST anomalies referenced to the *Control* period (1900-1999), obtained

487 by applying an EOF analysis to rainfall anomalies in the equatorial region (5°S-5°N, 140°E-
488 280°E). Note the different vector scales in **a** and **b**. Trends in the associated time series are
489 removed quadratically. The associated pattern and wind stress vectors beyond the domain are
490 obtained by a linear regression onto the detrended principal component. Colour scale
491 indicates SST in °C per one s.d. change; blue or red contours indicate cold or warm rainfall.
492 **c, d,** A nonlinear relationship between the first and second principal component for the
493 *Control* (1900-1999) and *Climate Change* (2000-2099) periods. An extreme La Niña event
494 (**red** dots) is defined as when the first principal component is greater than 1 and when the
495 second principal component is greater than 0.75 s.d.. An extreme El Niño event (**red** dots) is
496 defined as when amplitude of the first principal component is greater than 1, and when the
497 second principal component is greater than 0.75 s.d.. Number of extreme El Niño and La
498 Niña years is indicated.
499

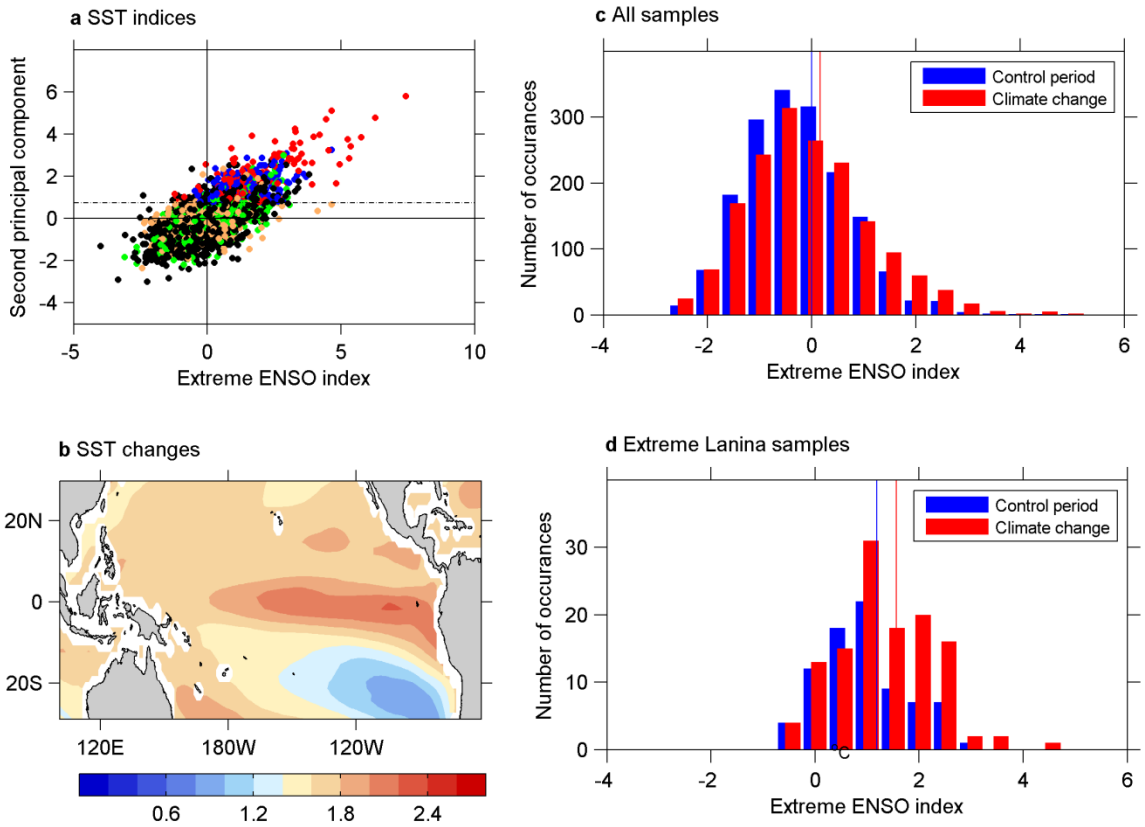

500

Figure 4 | Multi-model statistics associated with the increase in frequency of extreme La Niña events. **a,** Relationship between principal component of the second SST variability pattern and time series of ENSO extreme Amplifier, defined as an average over the east (5^oS-5^oN, 80^oW-90^oW) minus that over the central Pacific (5^oS-5^oN, 160^oE-210^oE). **b,** Multi-model ensemble average of SST changes (in ^oC) between the average over the *Climate Change* and the *Control* period. **c**, **d**, Multi-model ensemble histogram of ENSO raw Amplifier index but normalised by the standard deviation of the *Control* period for all samples and for extreme La Niña samples only, respectively. Values are separated into 0.5 bins centred at the tick point for the *Control* (**blue**) and *Climate Change* (**red**) period. The multi-model median for the *Control* (dashed **blue** line) and the *Climate Change* (dashed **red** line) periods are indicated. An extreme La Niña event (**blue** dots) is defined as when the first principal component is greater than 1.0 standard deviation (s.d.), and the second principal component is greater than 0.75 s.d. An extreme El Niño event (**red** dots) is defined as when amplitude of the first principal component is greater than 1.0 standard deviation (s.d.), and the second principal component is greater than 0.75 s.d. **Orange** dots indicate **weak El Niño**, and **green** dots, **weak La Niña** defined as when quadratically detrended Niño3 is greater than 0.75 s.d. in amplitude.